Optical excitations of polyacenes and bacteriochlorophyll-A using a GW and Bethe-Salpeter equation approach in the Exciton code

C. H. Patterson
School of Physics, Trinity College Dublin, Dublin 2, Ireland
(Dated: October 9, 2018)

The GW and Bethe-Salpeter Equation (BSE) approaches to solving optical excitation problems are well known in condensed matter theory and are becoming established also in molecular physics. We present results of optical excitation calculations of polyacenes from naphthalene to hexacene and a bacteriochlorophyll-A chromphore from the purple bacterium, *Rhodospirillum molischianum*, using new G_oW_o and Bethe-salpeter equation BSE modules in the Exciton code. Four-center screened and unscreened Coulomb matrix elements are calculated using a resolution of the identity approach. Scaling of time taken in integral generation, Hamiltonian assembly and diagonalization and convergence of excitation energies with respect to the dimension of the active space and number of random phase approximation modes included in screening are discussed.

PACS numbers: 31.10.+z, 31.15.ag, 33.20.Lg

I. INTRODUCTION

A combined GW and Bethe-Salpeter equation (BSE) approach provides a good compromise between accuracy and computational expense in the calculation of optical properties of large molecules, compared with accurate but expensive quantum chemistry methods such as coupled cluster (CC) theory or less accurate, inexpensive density functional theory (DFT) methods. It has been widely applied to periodic systems where the non-interacting Green's function, G_o, is conventionally obtained from a DFT or hybrid DFT calculation. Hartree-Fock (HF) exchange in solids is computationally expensive and in metals or narrow band gap systems there is an added difficulty of non-analytic behavior at small wave vector (long range in real space). Consequently range-separated hybrid DFT functionals are commonly used in periodic system calculations. Furthermore, HF exchange is largely screened in narrow gap periodic systems. Hence a DFT non-interacting Green's function is appropriate in these systems. In organic molecules, however, screening of HF exchange is weaker and a HF non-interacting Green's function is more appropriate.

Low energy optical excitations in polyacenes and porphyrins may be understood in terms of a small number of excitations between occupied and virtual states close to the HOMO and LUMO. Schmidt[1] proposed a model for optical excitations in polyacenes which involves the HOMO, LUMO and states one below the HOMO (H-1) and one above the LUMO (L+1). This model is shown to be valid in the BSE approach used here. Gouterman[2] proposed a model for low energy excitations in porphyrins which is used to interpret BSE calculations on bacteriochlorophyll-A (BChla). Quantum chemical calculations of optical excitations in chlorophylls and bacteriochlorophylls have been reviewed[3].

Several groups have developed Gaussian orbital GW and BSE codes[4–6] and recently this approach has been benchmarked for organic molecules using hybrid DFT non-interacting Green's functions[7–9]. Here we report GW and BSE calculations of ionization potentials (IP), electron affinities (EA) and optical excitations of well-studied polyacene systems[5,8,10–13] and a large biological chromophore, BChla. Calculations were performed using a new module in the Exciton code[14]. The algorithm[15] used for solving the generalized eigenvalue problem which arises in BSE and time-dependent Hartree-Fock (TDHF) calculations, the resolution of the identity (RI) algorithm[16–19] used for calculating four center Coulomb integrals and convergence of low lying excitations in tetracene with respect to active space dimensions are described in Supporting Information. The RI algorithm results in large savings in computational effort in transformation of Coulomb integrals from the atomic basis set to the molecular orbital (MO) basis. For a large molecule the number of three center Coulomb integrals which need to be transformed is still very large and we describe a distribution of these integrals over processor cores which allows the algorithm to scale for large molecules.

It is shown that perturbative G_oW_o calculations using a HF non-interacting Green's function (G_oW_o@HF, this work) and using an optimally tuned range-separated hybrid functional (G_oW_o@OTRSH[8]) non-interacting Green's function yield IP and EA in comparable agreement with accurate CCSD(T) calculations for the polyacene series[8]. It has been noted previously that G_oW_o@HF calculations on organic molecules yield similar IP and EA to GW@HF calculations where self-consistency in the single-particle energies in the Green's function has been achieved[5]. Furthermore, the HOMO-LUMO gap from HF calculations on porphin is within several tenths of an eV of the GW HOMO-LUMO gap while the gap obtained in a local density approximation (LDA) DFT calculation differs from the GW gap by over 3 eV[20]. Comparisons are also made between predictions of low-energy optical excitations in the polyacenes from full BSE calculations and the Tamm-Dancoff approximation to BSE (BSE-TDA) using either a G_oW_o@HF (this work) or a G_oW_o@BHLYP[21] non-interacting Green's function.

The most computationally expensive part of a BSE calculation is evaluation of the screened interaction needed in both the G_oW_o self-energy and BSE screened electron-hole interaction. Convergence of IP, EA and optical excitation energies depends on basis set, the number of HF virtual states included in the active space and the number of random phase approximation (RPA) modes included in the screened interaction in both G_oW_o and BSE calculations. For low energy excitations almost all of the screening is obtained using RPA modes with an energy cutoff in the virtual state space around 60 eV. Using only these modes in screening significantly reduces the cost of assembling the Hamiltonian in a BSE calculation on a large molecule.

In the following sections, the theoretical formalism of the GW and BSE methods is outlined; G_oW_o and BSE results for IP, EA and optical excitations in polyacenes from naphthalene to hexacene and BChla are compared to relevant results from similar methods and experiment; BSE calculations for polyacenes and BChla are reported and analyzed in terms of the model for optical excitations by Schmidt[1] and Gouterman[2], respectively.

II. THEORY

Excitations in molecules and solids are commonly calculated using methods based on the polarization propagator or density-density correlation function. Its poles occur at excitation energies and optical susceptibilities can be derived from it. The random phase approximation (RPA), time-dependent Hartree-Fock (TDHF) and Bethe-Salpeter equation (BSE) approximations to the polarization propagator are considered here. The TDHF approximation can be derived using the equation of motion for the HF density matrix[22,23] and the BSE approach is commonly derived using the equation of motion for the many-body one-particle Green's function[24]. The resulting equations are generalized eigenvalue problems. The non-Hermitian Hamiltonian matrix in each case consists of square $\mathbf{A}$ and $\mathbf{B}$ blocks. The various methods mentioned differ in whether or not electron-hole attraction terms are included (RPA versus TDHF) and whether or not the electron-hole interaction is screened (TDHF versus BSE). We begin by reviewing the TDHF equations using an approach by Dreuw and Head-Gordon[23] and similar notation.

A. Time-dependent HF approximation and linear response

The TDHF approximation for linear response to a time-dependent perturbation $V\cos(\omega t)$ can be derived[22,23,25] by assuming an order by order linear response of the density matrix,

$$\mathbf{P}(t) = \mathbf{P}^0 + \mathbf{P}^1(t)$$

so that the Fock matrix, $\mathbf{F}(t)$, which contains a time-independent self-consistent field part, $\mathbf{F}^0$, and a time-dependent part, is

$$\mathbf{F}(t) = \mathbf{F}^0 + \mathbf{F}^1(t),$$
$$\mathbf{F}^1(t) = \mathbf{V}(t) + \frac{\partial \mathbf{F}^0}{\partial \mathbf{P}}\mathbf{P}^1(t).$$

Here the density matrix is represented in the basis of eigenfunctions of $\mathbf{F}^0$, ψ_i and ψ_a, (i and a indices refer to occupied and virtual states, respectively). The first order change in the density matrix, $\mathbf{P}^1(t)$, contains only off-diagonal elements between occupied-virtual state pairs[23] and is represented as $P^1_{ai} = \frac{1}{2}(X_{ai}e^{-i\omega t} + Y^*_{ai}e^{+i\omega t})$. Here X_{ai} is an excitation amplitude and Y_{ai} is a deexcitation amplitude. Density matrix amplitudes, X_{ai} and Y_{ai}, are multiplied by $\psi_a(\mathbf{r})\psi^*_i(\mathbf{r})$ and $\psi_i(\mathbf{r})\psi^*_a(\mathbf{r})$, respectively, to generate the corresponding density. The perturbation in this basis is $V_{ai} = \frac{1}{2}(f_{ai}e^{-i\omega t} + f^*_{ia}e^{+i\omega t})$, where $f_{ai} = < a|V|i >$. Substitution of the perturbed density matrix into the equation of motion,

$$i\frac{\partial \mathbf{P}(t)}{\partial t} = [\mathbf{F}, \mathbf{P}], \tag{1}$$

yields the following set of linear response equations[22,23],

$$\begin{pmatrix} \mathbf{A} & \mathbf{B} \\ \mathbf{B}^* & \mathbf{A}^* \end{pmatrix}\begin{pmatrix} \mathbf{X} & \mathbf{Y}^* \\ \mathbf{Y} & \mathbf{X}^* \end{pmatrix} = \begin{pmatrix} \mathbf{1} & \mathbf{0} \\ \mathbf{0} & \mathbf{-1} \end{pmatrix}\begin{pmatrix} \mathbf{X} & \mathbf{Y}^* \\ \mathbf{Y} & \mathbf{X}^* \end{pmatrix}\begin{pmatrix} \mathbf{\Omega} & \mathbf{0} \\ \mathbf{0} & \mathbf{-\Omega} \end{pmatrix} - \begin{pmatrix} \mathbf{f} & \mathbf{f}^* \\ \mathbf{f} & \mathbf{f}^* \end{pmatrix}. \tag{2}$$

These equations may be abbreviated as $\mathbf{H}\xi = \mathbf{C}\xi\mathbf{\Omega} + \mathbf{D}$ in an obvious notation. The matrix,

$$\xi = \begin{pmatrix} \mathbf{X} & \mathbf{Y}^* \\ \mathbf{Y} & \mathbf{X}^* \end{pmatrix}, \tag{3}$$

contains first order density matrix amplitudes: $X_{ia} = d_{ia}$ and $Y_{ia} = d_{ai}$. Elements of the $\mathbf{A}$ and $\mathbf{B}$ matrices are given in Table I. Factors of two in Table I arise from summation over spin degrees of freedom. Chemists' notation for Coulomb matrix elements in the MO basis is used,

$$(ai|bj) = \int d\mathbf{r}d\mathbf{r}'\psi_a^*(\mathbf{r})\psi_i(\mathbf{r})\frac{1}{|\mathbf{r}-\mathbf{r}'|}\psi_b^*(\mathbf{r}')\psi_j(\mathbf{r}').$$

TABLE I. Table of matrix elements of A and B blocks of the Hamiltonian, H, for HF, RPA, TDHF and BSE approximations for a spin singlet molecule. Factors of two arise from summation over spin, tildes on energy eigenvalues for BSE indicate G_oW_o@HF eigenvalues and W_d is the dynamic part of the screened interaction, W_o

Method	
HF A	$(\epsilon_a-\epsilon_i)\delta_{ij}\delta_{ab}$
HF B	0
RPA A	$(\epsilon_a-\epsilon_i)\delta_{ij}\delta_{ab}$ + 2 (ai|jb)
RPA B	2 (ai|bj)
TDHF A	$(\epsilon_a-\epsilon_i)\delta_{ij}\delta_{ab}$ + 2 (ai|jb) - (ab|ji)
TDHF B	2 (ai|bj) - (aj|bi)
BSE A	$(\widetilde{\epsilon_a}-\widetilde{\epsilon_i})$ + 2 (ai|bj) - (ab|W_d|ji)
BSE B	2 (ai|bj) - (aj|W_d|bi)

In the absence of an external perturbation, the corresponding homogeneous equations,

$$\mathbf{H}\xi^o = \mathbf{C}\xi^o\mathbf{\Omega}^o, \tag{4}$$

are a pair of generalized eigenvalue problems,

$$\mathbf{H}\begin{pmatrix}\mathbf{X}^\alpha\\ \mathbf{Y}^\alpha\end{pmatrix} = \mathbf{C}\begin{pmatrix}\mathbf{X}^\alpha\\ \mathbf{Y}^\alpha\end{pmatrix}\Omega_+^\alpha,$$
$$\mathbf{H}\begin{pmatrix}\mathbf{Y}^{*,\alpha}\\ \mathbf{X}^{*,\alpha}\end{pmatrix} = \mathbf{C}\begin{pmatrix}\mathbf{Y}^{*,\alpha}\\ \mathbf{X}^{*,\alpha}\end{pmatrix}\Omega_-^\alpha,$$

where eigenvalues (labelled α) are in positive and negative pairs, where $\Omega_-^\alpha = -\Omega_+^\alpha$, and eigenvectors are chosen to have the norm condition,

$$\mathbf{X}^{*\alpha}\mathbf{X}^\beta - \mathbf{Y}^{*\alpha}\mathbf{Y}^\beta = \pm\delta_{\alpha\beta}, \tag{5}$$

where the sign of $\pm$ is the sign of the eigenvalue, $\Omega_\pm^\alpha$. $\mathbf{H}$ can therefore be expressed as $\mathbf{H} = \mathbf{C}\xi^o\mathbf{\Omega}^o\xi^{o,-1}$ with inverse,

$$\mathbf{H}^{-1} = \xi^o\mathbf{\Omega}^o\xi^{o,-1}\mathbf{C}^{-1}. \tag{6}$$

The inverse $(\mathbf{C}\omega-\mathbf{H})^{-1}$ is $\xi^o(\omega-\mathbf{\Omega}^o)^{-1}\xi^{o,-1}\mathbf{C}^{-1}$, where ω is a diagonal matrix with the dimension of the $\mathbf{A}$ matrix and contains the frequency of any perturbing potential. The inverse of $\mathbf{C}\omega-\mathbf{H}$ required to solve the inhomogeneous problem in Eq. 2 is,

$$\begin{pmatrix}\mathbf{X} & \mathbf{Y}^*\\ \mathbf{Y} & \mathbf{X}^*\end{pmatrix}\begin{pmatrix}\omega-\mathbf{\Omega}_+^o+i\eta\mathbf{1} & \mathbf{0}\\ \mathbf{0} & \omega+\mathbf{\Omega}_+^o-i\eta\mathbf{1}\end{pmatrix}^{-1}\begin{pmatrix}\mathbf{X}^* & \mathbf{Y}^*\\ -\mathbf{Y} & -\mathbf{X}\end{pmatrix}. \tag{7}$$

Sign pairing of eigenvalues has been used to rewrite the bottom right block of the inverse in Eq. 7, -$(\mathbf{\Omega}^o)_-$, as +$(\mathbf{\Omega}^o)_+$. Infinitesimal imaginary parts have been added to shift the poles off the real axis. The product $\xi^{o,-1}\mathbf{C}$ is,

$$\begin{pmatrix}\mathbf{X}^* & -\mathbf{Y}^*\\ -\mathbf{Y} & \mathbf{X}\end{pmatrix}\begin{pmatrix}\mathbf{1} & \mathbf{0}\\ \mathbf{0} & -\mathbf{1}\end{pmatrix} = \begin{pmatrix}\mathbf{X}^* & \mathbf{Y}^*\\ -\mathbf{Y} & -\mathbf{X}\end{pmatrix}. \tag{8}$$

Explicit evaluation of the inverse in Eq. 7 yields the density-density response matrix,

$$\begin{pmatrix}\mathbf{X}\\ \mathbf{Y}\end{pmatrix}\left(\omega-\mathbf{\Omega}_+^\alpha+i\eta\mathbf{1}\right)^{-1}\begin{pmatrix}\mathbf{X}^* & \mathbf{Y}^*\end{pmatrix} - \begin{pmatrix}\mathbf{Y}^*\\ \mathbf{X}^*\end{pmatrix}\left(\omega+\mathbf{\Omega}_-^\alpha-i\eta\mathbf{1}\right)^{-1}\begin{pmatrix}\mathbf{Y} & \mathbf{X}\end{pmatrix} \tag{9}$$

where the particular approximation depends on the $\mathbf{A}$ and $\mathbf{B}$ matrices in Table I. The density-density response function is obtained from it by multiplying the response matrix by products of eigenfunctions of the Fock operator, $\psi_a(\mathbf{r})\psi_i^*(\mathbf{r})$ and $\psi_i(\mathbf{r})\psi_a^*(\mathbf{r})$. In the HF case (Table I) where all off-diagonal elements of the $\mathbf{A}$ and $\mathbf{B}$ matrices are zero, the $\mathbf{X}$ matrix becomes the unit matrix, $\mathbf{Y}$ is zero and the HF polarizability is,

$$\frac{\mathbf{X}^\alpha\mathbf{X}^{\alpha,*}}{\omega-\Omega_+^\alpha+i\eta} - \frac{\mathbf{X}^{\alpha,*}\mathbf{X}^\alpha}{\omega+\Omega_+^\alpha-i\eta} \tag{10}$$

or,

$$\Pi^{HF}(\mathbf{r},\mathbf{r}';\omega) = \frac{\psi_a(\mathbf{r})\psi_i^*(\mathbf{r})\psi_a^*(\mathbf{r}')\psi_i(\mathbf{r}')}{\omega-(\epsilon_a-\epsilon_i)+i\eta} - \frac{\psi_a^*(\mathbf{r})\psi_i(\mathbf{r})\psi_a(\mathbf{r}')\psi_i^*(\mathbf{r}')}{\omega+(\epsilon_a-\epsilon_i)-i\eta}. \tag{11}$$

In the case of finite systems where orbitals and vectors in $\mathbf{X}$ and $\mathbf{Y}$ matrices are real, the density response matrix

simplifies to,

$$(\mathbf{X}+\mathbf{Y})\left[\left(\omega-\mathbf{\Omega}_{+}^{\alpha}+i\eta\mathbf{1}\right)^{-1}-\left(\omega+\mathbf{\Omega}_{+}^{\alpha}-i\eta\mathbf{1}\right)^{-1}\right](\mathbf{X}+\mathbf{Y})^{T} \tag{12}$$

B. Bethe-Salpeter equation and Tamm-Dancoff approximation

The matrix form of the BSE is analogous to the TDHF approximation with the exception that the electron-hole interaction in the BSE is dynamically screened and that, in a combined G_oW_o/BSE approach, the HF single-particle excitation energies, $\epsilon_a - \epsilon_i$, which appear in the **A** matrix of TDHF (Table I) are replaced by differences in the quasi-particle energies from a G_oW_o calculation, $\widetilde{\epsilon_a} - \widetilde{\epsilon_i}$. The screened interaction, W_o, which appears in a BSE calculation is energy dependent so that Eq. 2 can no longer be reduced to a generalized eigenvalue problem unless W_o is assumed to be energy-independent. This assumption has been made widely in solving the BSE[26] for periodic and molecular systems and we also adopt the approach where W_o is replaced by its static value. Solving the BSE problem is therefore similar to solving the TDHF problem, except that matrix elements of W_o must be obtained in addition to the bare Coulomb potential.

The Tamm-Dancoff approximation (TDA)[27]to either BSE or TDHF equations consists of omitting the **B** matrix from Eq. 2. In this case, the generalized eigenvalue problem becomes a standard, hermitian eigenvalue problem with the same dimension and elements as the **A** matrix in the BSE generalized eigenvalue problem. The method[15] used for solving the generalized eigenvalue problem is given in Supporting Information.

C. RPA polarizability and screened interaction

The self-energy operator, $\Sigma(\mathbf{r},\mathbf{r}';\epsilon)$, in many-body theory replaces the exchange correlation potential in DFT or the Fock exchange in HF theory by a dynamically screened exchange interaction. The G_oW_o approximation to the self-energy has been widely applied to periodic systems where it is conventional to express the screened interaction, W_o, in terms of the random phase approximation (RPA) inverse dielectric function and bare Coulomb potential[28]. A formally equivalent approach is to express W_o as,

$$W_o(\mathbf{r},\mathbf{r}',\epsilon) = v(\mathbf{r}-\mathbf{r}') + \int d\mathbf{r}''d\mathbf{r}'''v(\mathbf{r}-\mathbf{r}'')\Pi^{RPA}(\mathbf{r}'',\mathbf{r}''';\epsilon)v(\mathbf{r}'''-\mathbf{r}'), \tag{13}$$

where v is the bare Coulomb potential and Π^{RPA} is the RPA polarizability[27], obtained from Eq. 12 with **A** and **B** matrices for RPA given in Table I. The bare Coulomb term on the right hand side of Eq. 13 contributes the static HF exchange part of the self-energy and the second term is responsible for dynamic screening. Insertion of factors $\psi_a(\mathbf{r})\psi_i^*(\mathbf{r})$ into the density-density response matrix (Eq. 12) to yield the RPA polarizability and integration over $\mathbf{r}''$ and $\mathbf{r}'''$ in Eq. 13 yields the matrix representation,

$$W_{ai,bj} = (ai|bj) + \sum_{\alpha} w_{ai}^{\alpha} w_{bj}^{\alpha}\left(\frac{1}{\omega-\Omega_{+}^{\alpha}+i\eta} - \frac{1}{\omega+\Omega_{+}^{\alpha}-i\eta}\right) \tag{14}$$

where

$$w_{ai}^{\alpha} = (ai|ck)(X_{ck}^{\alpha}+Y_{ck}^{\alpha}). \tag{15}$$

D. G_oW_o approximation

Diagonal elements of the self-energy are obtained from convolution of the HF Green's function with the screened interaction along the real energy axis,

$$\Sigma(\mathbf{r},\mathbf{r}';\epsilon) = i\int_{-\infty}^{+\infty}\frac{d\epsilon'}{2\pi}e^{-i\epsilon'\eta}G_o(\mathbf{r},\mathbf{r}';\epsilon-\epsilon')W_o(\mathbf{r},\mathbf{r}',\epsilon) \tag{16}$$

Residues of the poles of G_o times the bare Coulomb potential in W_o are $\psi_i(\mathbf{r})\psi_i^*(\mathbf{r}')v(\mathbf{r}-\mathbf{r}')$ and diagonal matrix elements of this term in the self-energy are HF exchange matrix elements. These are included in the HF Hamiltonian and hence must be omitted from the self-energy. Only the latter, dynamic part of the screened interaction contributes to the self-energy. Note that the form of the self-energy in Eq. 16 is closely analogous to the self-energy obtained using a plasmon-pole approximation to the inverse dielectric function[28]. However, in the present case, no approximation to the RPA screened interaction is made since the RPA polarizability matrix is obtained exactly. Residues of W_d contribute the following diagonal matrix elements to the self-energy operator for occupied or virtual states,

$$\Sigma_{kk}(\omega) = \sum_{\alpha}\left(\frac{w_{ki}^{\alpha}w_{ik}^{\alpha}}{\omega-\epsilon_i+\Omega_{+}^{\alpha}-i\eta} + \frac{w_{ka}^{\alpha}w_{ka}^{\alpha}}{\omega-\epsilon_a+\Omega_{+}^{\alpha}+i\eta}\right). \tag{17}$$

Finally, the self-energy which is used to calculate shifts in

HF eigenvalues is multiplied by the quasi-particle weight function, $Z_{kk}(\omega) = (1 - \frac{\partial \Sigma_{kk}}{\partial \epsilon})^{-1}$.

III. RESULTS

In this section ionization potentials, electron affinities and optical excitations of acenes are compared to experimental data and previous BSE, BSE-TDA and CCSD(T) calculations. For BChla, ionization potentials, electron affinities and optical excitations are reported, and the optical absorption spectrum from a BSE-TDA calculation is compared to the UV-vis spectrum of monomeric BChla obtained in methanol. All molecular structures used in these calculations were relaxed using a B3LYP Hamiltonian and a 6-311G* Gaussian basis. Details of basis sets used for BSE calculations are given in Supporting Information.

A. Polyacenes

The transition dipole moment in low energy optical excitations of acenes lies in the molecular plane. Excitations are polarized either along the short or long in-plane axes. The x, y and z molecular axes in this work are oriented along the long in-plane, short in-plane and perpendicular directions, respectively. This orientation is used by Sony and Shukla[11]. Schmidt[1] chose the y axis along the long in-plane direction and x along the short in-plane direction. The two lowest optical excitations with light polarized along the short, y, axis were denoted p and β' by Clar[29] and ^1L_a and ^1B_a by Klevens and Platt[30]. The two lowest excitations with light polarized along the long, x, axis were denoted α and β[29] and ^1L_b and ^1B_b[30]. The transition charge density in the former two excitations is of B_{2u} symmetry and of B_{3u} symmetry for the latter two excitations. The lowest excitations of either symmetry type are denoted 1 B^+_{2u} and 1 B^-_{3u} in the work of Sony and Shukla[11].

1. Electronic configuration and excitations

Schmidt[1] explained the excited wavefunction character and optical activity of low energy dipole-active transitions in alternant hydrocarbons using a Hückel theory model consisting of single particle transitions between HOMO (H), LUMO (L) and H+1 and L-1 orbitals (Fig. 1), which is largely borne out by the calculations presented here. Single particle transitions among the four frontier orbitals generate four singly-excited determinants. Pairing of virtual and occupied orbital Hückel energies (Fig. 1) leads to two degenerate excitations with energy, (x + y)t, (where ϵ and t are Hückel on-site and hopping parameters and x and y are numbers that arise from diagonalization of the Hückel parameterized Hamiltonian) and two non-degenerate excitation energies (2xt and 2yt)[1].

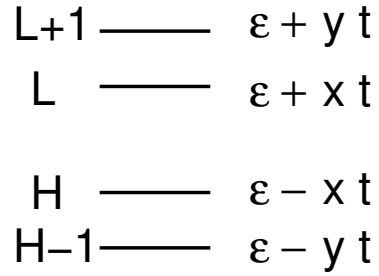

FIG. 1. Single-particle orbitals and paired Hückel orbital energies in an alternant hydrocarbon.

In-phase and out-of-phase linear combinations of the degenerate transitions (H $\rightarrow$ L+1 and H-1 $\rightarrow$ L) yield two excitations, the α and β states of Clar[29]. Transition moments from these two excited determinants combine in phase in the β excitation and it acquires almost all of the dipole activity. Splitting of these excitations exceeds 1 eV when interaction effects are included and the transition dipole is in the long, x, direction. Non-degenerate transitions in the single-particle frontier orbital picture are the H $\rightarrow$ L and H-1 $\rightarrow$ L+1 transitions. The former is the p excitation of Clar[29] and the latter is the β' excitation.

Schmidt reported photoelectron spectra and optical transition energies of 52 polynuclear aromatic hydrocarbons including polyacenes and obtained a correlation between their first and second ionization potentials and the ordering of low energy optical excitations[1]. He defines two cases, A and B, in which the difference in first and second ionization potentials is at least 0.7 eV (A) or less than 0.5 eV (B). In the former case, the ordering of optical excitations is $p < \alpha < \beta < \beta'$. In the latter case the splitting of the α and β excitations increases so that the order becomes $\alpha < p < \beta' < \beta$. Acenes from naphthalene to hexacene belong to category A according to Schmidt's photoelectron data[1] and from results of G_oW_o@HF calculations presented below. The predicted sequence of excitations for anthracene to hexacene is $p < \alpha < \beta < \beta'$ from BSE-TDA calculations presented below and from available experimental data (see below). Naphthalene is a marginal case with an experimental difference in the first and second IP's of 0.72 eV and a calculated difference of 0.69 eV. In this case the order of excitations is found to be $\alpha < p < \beta < \beta'$ from BSE-TDA calculations and $\alpha < p < \beta$ from Schmidt's data.

2. IP, EA and IP - EA values

Calculations on polyacenes were performed using cc-pVTZ and cc-pVTZ-RI basis sets. These and the dimensions of active spaces used in calculations are described in more detail in Supporting Information. Table II com-

TABLE II. HF (left column) and G_oW_o (right column) eigenvalues in eV and D_{2h} irreducible representations of HF orbitals which form dominant configurations of low-lying excited states in acenes. Orbitals with negative (positive) HF eigenvalues are occupied (unoccupied) in the HF ground state.

$C_{10}H_8$			$C_{14}H_{10}$			$C_{18}H_{12}$			$C_{22}H_{14}$			$C_{26}H_{16}$	
								b_{3g}	-9.55	-9.37	a_u	-8.93	-8.79
b_{3g}	-10.48	-10.33	a_u	-9.44	-9.43	b_{3g}	-8.60	-8.71	b_{2g}	-8.16	-8.37	b_{1u}	-8.09	-8.23
b_{1u}	-8.66	-8.95	b_{2g}	-8.42	-8.68	b_{1u}	-8.26	-8.52	a_u	-7.95	-8.10	b_{3g}	-7.43	-7.60
a_u	-7.86	-8.26	b_{3g}	-7.03	-7.50	a_u	-6.46	-6.99	b_{3g}	-6.05	-6.57	a_u	-5.73	-6.23
b_{2g}	2.31	0.77	b_{1u}	1.44	-0.08	b_{2g}	0.82	-0.69	b_{1u}	0.37	-1.08	b_{2g}	0.03	-1.35
b_{3g}	3.09	1.48	a_u	2.84	1.16	b_{3g}	2.67	0.93	b_{2g}	2.41	0.65	b_{1u}	1.85	0.19
a_g	3.96	3.15	b_{2g}	3.84	2.00	b_{1u}	3.08	1.24	a_u	2.55	0.82	b_{3g}	2.47	0.77

TABLE III. Comparison of *GW* IP and EA data with experiment and CCSD(T).

	$C_{10}H_8$	$C_{14}H_{10}$	$C_{18}H_{12}$	$C_{22}H_{14}$	$C_{26}H_{16}$	MAD
IP Expt.[a]	8.15	7.41	6.97	6.61	6.36	-
IP G_oW_o@HF[b]	8.26	7.50	6.99	6.57	6.23	0.03
IP G_oW_o@OTRSH[c]	8.35	7.57	7.03	6.65	6.38	0.08
IP CCSD(T)[c]	8.25	7.48	6.96	6.58	6.32	-
EA G_oW_o@HF[a]	-0.77	0.08	0.69	1.08	1.35	0.17
EA G_oW_o@OTRSH[c]	-0.28	0.56	1.15	1.58	1.90	0.32
EA CCSD(T)[c]	-0.48	0.28	0.82	1.21	1.47	-
IP - EA G_oW_o@HF[b]	9.03	7.42	6.30	5.49	4.88	0.17
IP - EA G_oW_o@OTRSH[c]	8.63	7.01	5.88	5.07	4.47	0.24
IP - EA CCSD(T)[c]	8.73	7.20	6.14	5.37	4.85	-

[a] Ref. [1]

[b] This work

[c] Ref. [8] Tables S7 and S10.

pares IP, EA and IP - EA energies for the polyacenes from Schmidt's photoelectron data, a CCSD(T) coupled cluster calculation[12] and G_oW_o calculations which started from Hartree-Fock wave functions and energy eigenvalues (G_oW_o@HF, this work) and optimally-tuned range-separated hybrid (G_oW_o@OTRSH) Hamiltonians[8]. IP values from G_oW_o@HF calculations are in very good agreement with values from CCSD(T) calculations. IP values from both G_oW_o@HF and G_oW_o@OTRSH calculations exceed those from CCSD(T), with the exception of G_oW_o@HF for pentacene and hexacene. Mean absolute deviations (MAD) of IP values for G_oW_o@HF and G_oW_o@OTRSH are 0.03 and 0.08 eV, respectively. G_oW_o@HF calculations of the EA, where the extra electron is bound, consistently underestimate CCSD(T) values with a MAD of 0.17 eV whereas G_oW_o@OTRSH calculations consistently overestimate these EA values with a MAD of 0.32 eV. Accuracy of IP - EA differences is critical for accurate prediction of optical excitations. IP - EA values from G_oW_o@HF are overestimated by 0.30 eV compared to CCSD(T) for naphthalene. Overestimation reduces steadily from napththalene to hexacene and values for both methods are in good agreement for hexacene. G_oW_o@OTRSH consistently underestimates IP - EA values compared to CCSD(T) by 0.10 eV for naphthalene and by 0.38 eV for hexacene. Overestimation of IP - EA values by a G_oW_o@HF and underestimation by hybrid DFT G_oW_o@OTRSH calculations is in agreement with generally accepted ideas regarding HF and DFT estimates of single-particle band gaps.

3. Low energy excitations

Low energy excitations in polyacenes studied in this work can mostly be accounted for using three or four occupied and three virtual orbitals. HF and G_oW_o@HF energy eigenvalues and orbital irreps for these orbitals are given in Table II. Table II shows that the order of states from H-2 to L+1 in naphthalene and tetracene is: $b_{3g} < b_{1u} < a_u < b_{2g} < b_{3g}$. The order of states from H-2 to H+2 in anthracene is $a_u < b_{2g} < b_{3g} < b_{1u} < a_u < b_{2g}$. In pentacene the order of the H-2 and H-1 and H+1 and H+2 levels are reversed to: $b_{2g} < a_u < b_{3g} < b_{1u} < b_{2g} < a_u$.

Dominant configurations in BSE-TDA excited state wave functions are given in Table III. The lowest, p, excitation in each case is predominantly the H $\rightarrow$ L transition whose weight increases from naphthalene to hexacene. The other short axis transition, β', should be dominated

TABLE IV. Dominant configurations in low energy excited states of acenes. Irreducible representations of transition density (TDI), transition dipole orientations (TDO) and weights of transitions from orbitals around the HOMO (H) and LUMO (L) are given.

TDI	TDO	$C_{10}H_8$				$C_{14}H_{10}$				$C_{18}H_{12}$				$C_{22}H_{14}$				$C_{26}H_{16}$			
p	y	H	→	L	0.89	H	→	L	0.94	H	→	L	0.96	H	→	L	0.96	H	→	L	0.97
β'	y	H-1	→	L+1	0.84	H	→	L+6	0.95	H	→	L+6	0.63	H-3	→	L	0.69	H-3	→	L	0.71
		H	→	L	-0.42					H-2	→	L+2	-0.47	H-1	→	L+1	0.51	H-1	→	L+1	0.52
α	x	H-1	→	L	0.70	H-1	→	L	0.71	H-1	→	L	0.71	H-2	→	L	0.72	H-2	→	L	0.71
		H	→	L+1	0.70	H	→	L+1	-0.68	H	→	L+1	-0.66	H	→	L+2	-0.64	H	→	L+2	0.66
β	x	H-1	→	L	0.68	H-1	→	L	0.67	H-1	→	L	0.66	H-2	→	L	0.64	H-2	→	L	0.60
		H	→	L+1	-0.69	H	→	L+1	0.70	H	→	L+1	0.71	H	→	L+2	0.72	H	→	L+2	0.75
1 B_{1g}	-	H	→	L+5	0.85	H-2	→	L	-0.74	H-2	→	L	-0.78	H-1	→	L	-0.83	H-1	→	L	0.84
		H-2	→	L	-0.46	H	→	L+2	0.62	H	→	L+2	0.57	H	→	L+1	0.53	H	→	L+1	0.50
2 B_{1g}	-	H-2	→	L	0.87	H-2	→	L	0.62	H-2	→	L	0.56	H-1	→	L	0.51	H-1	→	L	0.49
		H	→	L+5	0.49	H	→	L+2	0.74	H	→	L+2	0.77	H	→	L+1	0.82	H	→	L+1	-0.83

by the H-1 → H+1 transition according to Schmidt's model[1]. Table III shows that this is the dominant excitation in naphthalene and is an important excitation in pentacene and hexacene. However, other transitions of the same symmetry are more important in the β' state in other acenes. α and β excitations are linear combinations of H-1 → L and H → L+1 transitions for naphthalene to tetracene and linear combinations of the H-2 → L and H → L+2 transitions in pentacene and hexacene, owing to the switch in order of the H±1 and H±2 states in pentacene and hexacene, mentioned above.

Optically dark states whose transition charge density has B_{1g} (xy) symmetry occur at low energies, especially in pentacene and hexacene where they arise from $a_u \otimes b_{1u}$ and $b_{2g} \otimes b_{3g}$ orbital products. They arise from linear combinations of H-1 → L and H → L+1 transitions in pentacene and hexacene and H-2 → L and H → L+2 transitions in anthracene and tetracene. There is also a relatively low lying A_{1g} state in the same energy range as the β' excitation.

Table V presents results of BSE, BSE-TDA, CCSD(T) calculations and experimental values of optical excitation energies as well as low energy, B_{1g} and A_{1g} dipole-forbidden transitions. Data in the table show that the BSE approximation predicts significantly lower p excitation energies than CCSD(T). Experimental excitation energies presented in Table V are from Klevens and Platt[30], Biermann and Schmidt[31] and Schmidt[1]. According to Biermann and Schmidt, UV transitions were measured in solution and extrapolated to the gas phase by adding between 250 and 400 cm^{-1} (0.03 and 0.05 eV) to the vibrational 0-0 levels measured in solution for the α excitation and between 900 and 1500 cm^{-1} (0.11 and 0.19 eV) for the p and β excitation, the particular amount added depended on solvent. These corrected values are cited in Table V.

From Table V we see that there is mostly good agreement between BSE and BSE-TDA excitations which use G_oW_o@HF and G_oW_o@OTRSH non-interacting Green's functions. MAD values for the p and α excitation energies using BSE, BSE-TDA and the G_oW_o@HF and G_oW_o@OTRSH Green's functions are given at the bottom of Table V. Both BSE@HF and BSE@OTRSH methods underestimate the p excitation energy by around 0.5 eV, while BSE-TDA@HF and BSE-TDA@OTRSH methods underestimate it by around 0.2 eV. BSE@HF and BSE@OTRSH methods give a slightly better agreement with CCSD(T) than BSE-TDA@HF and BSE-TDA@OTRSH, with MAD values around 0.1 eV.

B. Bacteriochlorophyll-A

The structure of BChla ($C_{55}N_4O_6MgH_{74}$, Fig. 2) was obtained from the crystal structure of light harvesting complex II in the purple bacterium *Rhodospirilium molischianum*[32] (Protein Data Bank[33,34] PDB ID: 1LGH[32]). Molecular structures of membrane proteins such as 1LGH determined by x-ray crystallography have limited resolution. It is important therefore to relax the structure obtained from PDB before performing high level quantum chemical calculations. As noted above, all molecular structures used in these calculations were relaxed using a B3LYP Hamiltonian and 6-311G* Gaussian basis. HF molecular orbital energies in the experimental PDB structure shift down by up to 1 eV in the relaxed structure. Geometry changes which result from relax-

TABLE V. Low energy excitations in polyacenes from naphthalene to hexacene in eV from BSE, BSE-TDA and CCSD(T) calculations and experiment. TD is transition density.

Excitation	TD	BSE[a]	BSE[b]	TDA[a]	TDA[b]	CCSD(T)[c]	Expt.
			$C_{10}H_8$				
p	y	4.28	4.34	4.52	4.59	4.79	4.34[d], 4.38[e]
β'	y	5.91	-	6.37	-	-	-
α	x	4.26	4.30	4.39	4.32	4.13	3.97[d], 4.03[e]
β	x	5.76	-	6.29	-	-	5.62[e]
B_{1g}	xy	5.86	-	6.16	-	-	-
B_{1g}	xy	6.52	-	6.54	-	-	-
A_{1g}	-	6.13	-	6.20	-	-	-
			$C_{14}H_{10}$				
p	y	3.21	3.38	3.49	3.63	3.69	3.31[d], 3.38[e]
β'	y	5.54	-	5.85	-	-	5.73[f]
α	x	3.63	3.82	3.77	3.79	3.59	3.47[d], 3.57[e]
β	x	5.02	-	5.48	-	-	4.83[d], 4.86[d]
B_{1g}	xy	4.71	-	4.97	-	-	-
B_{1g}	xy	5.49	-	5.51	-	-	-
A_{1g}	-	5.50	-	5.56	-	-	-
			$C_{18}H_{12}$				
p	y	2.46	2.42	2.75	2.72	2.94	2.60[d], 2.71[e]
β'	y	4.86	-	5.11	-	-	-
α	x	3.21	3.33	3.36	3.37	3.25	3.16[d], 3.32[e]
β	x	4.50	-	4.90	-	-	4.55[d], 4.52[e]
B_{1g}	xy	3.80	-	4.06	-	-	-
B_{1g}	xy	4.64	-	4.66	-	-	-
A_{1g}	-	4.83	-	4.90	-	-	-
			$C_{22}H_{14}$				
p	y	1.92	1.88	2.25	2.21	2.42	2.14[d], 2.23[e]
β'	y	4.14	-	4.40	-	-	-
α	x	2.92	3.10	3.06	3.13	3.02	2.96[d], 3.05[e]
β	x	4.12	-	4.44	-	-	4.01[d], 4.14[e]
B_{1g}	xy	3.10	-	3.36	-	-	-
B_{1g}	xy	3.96	-	3.98	-	-	-
A_{1g}	-	4.31	-	4.37	-	-	-
			$C_{26}H_{16}$				
p	y	1.52	1.48	1.84	1.84	2.05	1.90[e]
β'	y	3.52	-	3.78	-	-	-
α	x	2.71	2.91	2.88	2.98	2.86	2.96[x], 2.80[e]
β	x	3.83	-	4.12	-	-	-
B_{1g}	xy	2.55	-	2.82	-	-	-
B_{1g}	xy	3.43	-	3.45	-	-	-
A_{1g}	-	3.90	-	3.99	-	-	-
p MAD		0.50	0.48	0.21	0.18	-	-
α MAD		0.09	0.12	0.12	0.15	-	-

[a]Ref. [This work],
[b]Ref. [13],
[c]Ref. [12],
[d]Ref. [30],
[e]Ref. [31],
[f]Ref. [1]

ation are mainly small changes in bond length or bond angle rather than gross changes in the molecular configuration. Electronic properties of chlorophyll species are commonly calculated without the aliphatic phytyl chain, which is not expected to participate in low energy optical excitations. It is included here to illustrate the capacity of the method implemented in the Exciton code.

1. *Gouterman model electronic structure*

Electronic structures of BChla, chlorophyll-a (Chla) and porphyrins differ in the number of π electrons, having 26, 24 and 22, respectively. BChla and porphyrins therefore conform to the 4n + 2 aromaticity rule, while Chla does not. The model of Gouterman[2] explained four low energy excitations in porphyrins, denoted Q_x, Q_y, B_x and B_y, in terms of four frontier orbitals. In an ideal D_{4h} symmetry these are occupied a_{1u} and a_{2u} orbitals and a degenerate e_g pair of virtual orbitals. Direct products of both a_{1u} and a_{2u} with e_g are e_u, leading to two degenerate excitations of E_u symmetry with (x,y) transition moments (in this ideal symmetry case). In porphin (D_{2h}), the occupied frontier orbitals belong to b_{2g} and b_{3g} irreps and virtual frontier orbitals belong to a_u and b_{1g} irreps. At the HF level the splitting of the b_{2g} and b_{3g} levels is 0.6 eV and splitting of the a_u and b_{1g} levels is 0.06 eV.

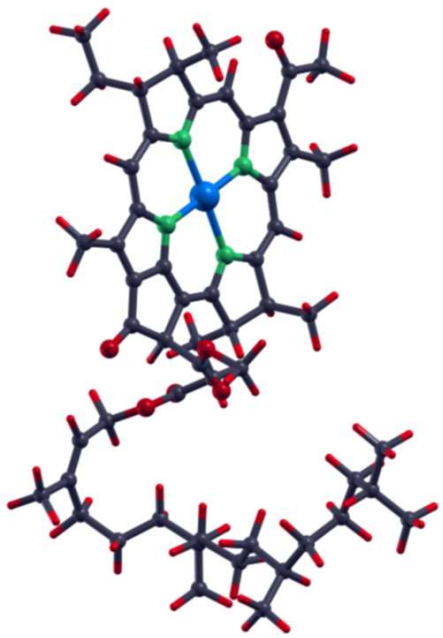

FIG. 2. Structure of BChla molecule derived from PDB 1LGH structure in Ref. [32].

2. *IP, EA and IP - EA values*

Calculations on BChla were performed using cc-pVDZ and cc-pVDZ-RI basis sets. These and the dimensions of active spaces used in calculations are described in more detail in Supporting Information. HF and G_oW_o eigenvalues for the four frontier orbitals in BChla are given in Table VI. The H and H -1 states in BChla are split by 1.6 eV and 1.2 eV in HF and G_oW_o calculations and the L and L + 1 states are split by 2.58 eV and 2.1 eV, respectively. There is only a minor change in IP, EA and IP - EA energies in BChla going from HF to G_oW_o methods, in marked contrast to the polyacenes (Table II). The IP - EA energy difference reduces from 4.72 to 4.41 eV on going from HF to G_oW_o.

3. *Low energy excitations*

Dominant configurations in four low energy excitations in BChla are given in Table VII and excitation energies are given in Table VIII. These are the Q_x and Q_y bands and the two B bands with the strongest dipole acivity in a group of bands around 4 eV, which are identified as the B_x and B_y bands in Gouterman's model[2]. In addition to these strongly dipole-active bands with x and y polarization, there are a number of additional bands in this range with lesser dipole activity. This was also found to be the case in a model Hamiltonian configuration interaction singles (CIS) calculation[3]. The Q_y excitation at 1.77 eV in a BSE-TDA calculation is an out-of-phase combination of H $\rightarrow$ L and H-1 $\rightarrow$ L+1 configurations. The Q_x excitation at 2.26 eV is an in-phase combination of H-1 $\rightarrow$ L and H $\rightarrow$ L+1. The B_x excitation at 4.10 eV is an out-of-phase combination of H $\rightarrow$ L+1 and H-1 $\rightarrow$ L and B_y is an in-phase combination of H-1 $\rightarrow$ L+1 and H $\rightarrow$ L. Linnanto and Korppi-Tommola[3] list excited state configurations for the Q_x, Q_y and one B band in BChla from a CIS calculation. These are given in Table VIII and agree well with configurations for these bands from a BSE-TDA calculation. Cai *et al.* report similar dominant configurations for corresponding excitations of Chla from a TD-DFT calculation[36], although configuration weights were not given.

The Q_x band position from a BSE calculation at 1.99 eV is underestimated by about 0.1 eV compared to ex-

TABLE VI. HF and G_oW_o eigenvalues in eV of frontier orbitals of BChla.

	HF	G_oW_o
H - 1	-7.05	-6.53
H	-5.46	-5.38
L	-0.73	-0.97
L + 1	1.85	1.13

TABLE VII. Dominant configurations in low energy excited states of BChla from BSE-TDA and model Hamiltonian configuration interaction singles (CIS) calculations. Transition dipole orientations (TDO) and weights of transitions are given.

	TDO		BSE-TDA[a]	CIS[b]
Q_y	y	H → L	0.90	0.94
		H-1 → L+1	-0.37	-0.29
Q_x	x	H-1 → L	0.84	0.76
		H → L+1	0.52	0.63
B_x	x	H → L+1	0.73	0.73
		H-1 → L	-0.47	-0.57
B_y	y	H-1 → L+1	0.65	
		H → L+5	0.41	
		H → L	0.25	

[a]This work
[b]Ref. [3]

periment (2.1 eV) while the Q_y band at 1.34 eV is underestimated by around 0.3 eV (compared to 1.6 eV). This comparison does not take solvent interactions into account, which may shift gas phase absorption frequencies downwards by 350 to 900 cm^{-1}[31] (0.04 to 0.1 eV), nor does it include shifts due to strong vibronic coupling

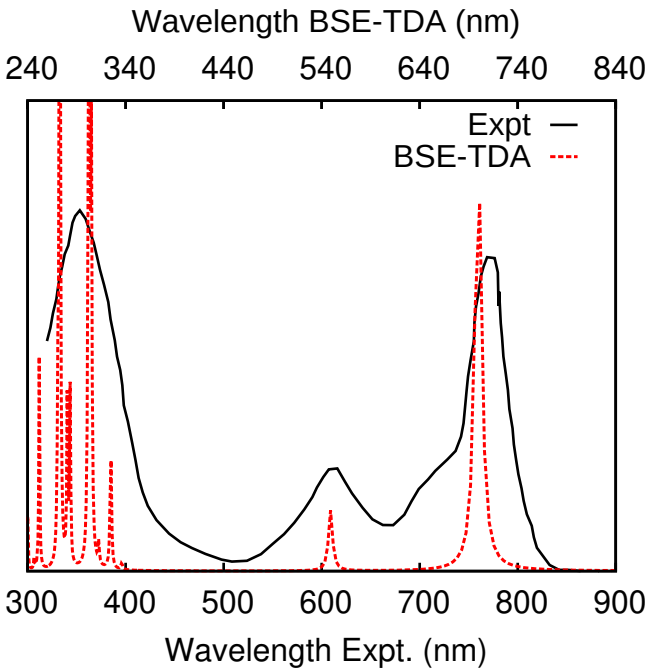

FIG. 3. Dipole approximation optical absorption spectrum for BChla molecule in 1LGH light harvesting complex from BSE-TDA calculation compared to spectrum from monomeric BChla in methanol solution, redrawn from Ref. [35].

between Q_x and Q_y bands[37]. TDHF-TDA Q_x and Q_y band positions are overestimated by 0.6 and 0.3 eV and the B_x and B_y band positions are overestimated by 1.2 to 1.8 eV. The BSE-TDA method therefore gives the best overall agreement with experimental excitation energies.

The optical absorption spectrum which is obtained from a BSE-TDA calculation is shown in Fig. 3, where it is compared to the UV-vis absorption spectrum measured for a monomeric solution of BChla[35]. The experimental spectrum shows Q_x and Q_y bands around 600 nm and 770 nm and a broad band around 350 nm. The shoulder on the 770 nm peak is most likely due to the 0-1 vibronic excitation of the 770 nm band and not an additional electronic transition. The BSE-TDA spectrum has Q_x and Q_y bands at 550 nm and 700 nm and B_x and B_y bands around 300 nm. The wavelength axis for the BSE-TDA calculation in Fig. 3 has been shifted relative to that for experiment by 60 nm.

IV. SUMMARY AND CONCLUSIONS

In summary, calculations of IP, EA and low energy excitations in polyacenes and BChla using HF, G_oW_o and BSE and related methods in the Exciton code[14] have been presented and analyzed in terms of frontier orbital models by Schmidt[1] and Gouterman[2]. Mean absolute deviations (MAD) of IP and EA energies from CCSD(T) calculations[8] are 0.03 eV for IP values and 0.17 eV for EA values, across the range of polyacenes studied. These values are lower than similar optimally tuned range separated hybrid (OTRSH) DFT calculations[8] (0.08 eV and 0.32 eV, respectively), showing that a G_oW_o@HF non-interacting Green's function is a good starting point for many-body calculations on conjugated organic molecules. Low energy optical excitations in polyacenes from BSE and BSE-TDA calculations are mostly in good agreement with BSE-TDA calculations which used a G_oW_o@OTRSH non-interacting Green's function[13]. The dominant single-particle transitions in the p, α, β and β' states from BSE-TDA calculations are in qualitative agreement with the model of Schmidt[1].

Similar calculations on BChla are presented and analyzed. Results of calculations are compared to the optical spectrum of monomeric BChla obtained in methanol[35].

TABLE VIII. Low energy excitations in BChla in eV from BSE, BSE-TDA, TDHF-TDA and optical absorption measurements.

	BSE [a]	BSE-TDA[a]	TDHF-TDA[a]	Expt.[b]
Q_y	1.34	1.77	1.90	1.6
Q_x	1.99	2.26	2.66	2.1
B_x	3.45	4.10	4.68	3.5
B_y	4.21	4.55	5.31	3.5

[a]This work
[b]Ref. [35]

The position of the Q_y bands is predicted by BSE calculations to be 0.3 eV lower than experimental positions. BSE-TDA calculations predict both Q_x and Q_y bands to be around 0.2 eV above experimental positions; TDHF-TDA calculations predict higher energies than BSE-TDA. The shape of the optical absorption spectrum of BChla is in good agreement with the experimental spectrum except for an overall shift of 60 nm.

Algorithms used for solving the generalized eigenvalue problem encountered in BSE and TDHF calculations[15] and the resolution of the identity method[16–19] implemented in the Exciton code are described in Supporting Information, along with a description of scaling of various parts of a BSE-TDA calculation with system size and the dependence of excitation energies on active space sizes and the number of RPA modes included in the screened Coulomb interaction.

ACKNOWLEDGMENTS

The author gratefully acknowledges discussions with A. Shukla and J. F. McGilp. Work on this project was initiated during a sabbatical visit to the Quantum Theory Project at the University of Florida, hosted by R. J. Bartlett. A. Elena of the STFC Hartree Centre, Daresbury, UK (then at the Irish Centre for High End Computing) gave assistance with some aspects of the code in its early development stages. Calculations were performed on the Boyle cluster maintained by the Trinity Centre for High Performance Computing, funded through grants from Science Foundation Ireland.

[1] W. Schmidt, J. Chem. Phys. **66**, 828 (1977).
[2] M. Gouterman, J. Mol. Spectrosc. **6**, 138 (1961).
[3] J. Linnanto and J. Korppi-Tommola, Phys. Chem. Chem. Phys. **8**, 663 (2006).
[4] M. Rohlfing, P. Krüger, and J. Pollmann, Phys. Rev. B **48**, 17791 (1993).
[5] X. Blase, C. Attaccalite, and V. Olevano, Phys. Rev. B **83**, 115103 (2011).
[6] F. Bruneval, T. Rangel, S. M. Hamed, M. Shao, C. Yang, and J. B. Neaton, Computer Phys. Comm. **208**, 149 (2016).
[7] D. Jacquemin, I. Duchemin, and X. Blase, J. Chem theory Comput. **11**, 3290 (2015).
[8] T. Rangel, S. M. Hamed, F. Bruneval, and J. B. Neaton, J. Chem. Theory Comput. **12**, 2834 (2016).
[9] C. Azarias, C. Habert, S. Budzák, X. Blase, and I. Duchemin, J. Phys. Chem. A **121**, 6122 (2017).
[10] E. S. Kadantsev, M. J. Stott, and A. Rubio, J. Chem. Phys. **124**, 134901 (2006).
[11] P. Sony and A. Shukla, Phys. Rev. B **75**, 155208 (2007).
[12] K. Lopata, R. Reslan, M. Kowalska, D. Neuhauser, N. Govind, and K. Kowalski, J. Chem. Theory Comput. **38**, 3686 (2011).
[13] T. Rangel, S. M. Hamed, F. Bruneval, and J. B. Neaton, J. Chem. Phys. **146**, 194108 (2017).
[14] C. H. Patterson, Mol. Phy. **108**, 3181 (2010).
[15] M. Shao, F. H. da Journada, C. Yang, J. Deslippe, and S. G. Louie, Linear Algebra Appl. **488**, 148 (2016).
[16] J. L. Whitten, J. Chem. Phys. **58**, 4496 (1973).
[17] E. J. Baerends, D. E. Ellis, and P. Ros, Chem. Phys. **2**, 41 (1973).
[18] H. Sambe and R. H. Felton, J. Chem. Phys. **62**, 1122 (1975).
[19] B. I. Dunlap, J. W. D. Connolly, and J. R. Sabin, J. Chem. Phys. **71**, 3396 (1979).
[20] C. Hogan, M. Palummo, J. Gierschner, and A. Rubio, J. Chem. Phys. **138**, 024312 (2013).
[21] A. D. Becke, J. Chem. Phys. **98**, 1372 (1993).
[22] Y. Öhrn, *Propagators in quantum chemistry*, 2nd ed. (Wiley, Hoboken, New Jersey, 2004).
[23] A. Dreuw and M. Head-Gordon, Chem. Rev. **105**, 4009 (2005).
[24] L. P. Kadanoff and G. Baym, *Quantum statistical mechanics: Green's function methods in equilibrium and non-equilibrium processes* (CRC Press, New York, 1962).
[25] A. D. McLachlan and M. A. Ball, Rev. Mod. Phys. **36**, 844 (1964).
[26] M. Rohlfing and S. G. Louie, Phys. Rev. Lett. **81**, 2312 (1998).
[27] A. L. Fetter and J. D. Walecka, *Quantum Theory of many-particle systems*, Vol. New York (McGraw-Hill, 1971).
[28] M. S. Hybertsen and S. G. Louie, Phys. Rev. B **34**, 5390 (1986).
[29] E. Clar, Ber. Deutsch Chem. Ges. **69**, 607 (1936).
[30] H. B. Klevens and J. R. Platt, J. Chem. Phys. **17**, 470 (1949).
[31] D. Biermann and W. Schmidt, J. Am. Chem. Soc. **102**, 3163 (1980).
[32] J. Koepke, X. Hu, C. Muenke, K. Schulten, and H. Michel, Structure **4**, 581 (1996).
[33] .
[34] H. M. Berman, J. Westbrook, Z. Feng, G. Gilliland, T. N. Bhat, H. Weissig, I. N. Shindyalov, and P. E. Bourne, Nucl. Acids Res. **28**, 235 (2000).
[35] J. Gottstein and H. Scheer, Proc. Natl. Acad. Sci. USA **80**, 2231 (1983).
[36] Z.-L. Cai, M. J. Crossley, J. R. Reimers, R. Kobayashi, and R. D. Amos, J. Phys. Chem. B **110**, 15624 (2006).
[37] J. R. Reimers, Z.-L. Cai, R. Kobayashi, M. Rätsep, A. Freiburg, and E. Krausz, Sci. Rep. **3**, 276 (2013).